TiO2 supported non-noble Ni-Fe catalysts for the high yield production of 2,5-dimethylfuran biofuel

Martyna Przydacz, Marcin Jędrzejczyk, Jacek Rogowski, Dris Ihiawakrim, Nicolas Keller, Agnieszka Ruppert

TiO_2 supported non-noble Ni-Fe catalysts for the high yield production of 2,5-dimethylfuran biofuel

Martyna Przydacz[a], Marcin Jędrzejczyk[a], Jacek Rogowski[a], Dris Ihiawakrim[c], Nicolas Keller[b], Agnieszka M. Ruppert[a]*

[a] Institute of General and Ecological Chemistry, Faculty of Chemistry, Lodz University of Technology, ul. Żeromskiego 116, 90-924 Lodz, Poland

[b] Institut de Chimie et Procédés pour l'Energie, l'Environnement et la Santé, CNRS/University of Strasbourg, 67087 Strasbourg, France

[c] Institut de Physique et Chimie des Matériaux de Strasbourg (IPCMS), CNRS/University of Strasbourg, 67034 Strasbourg, France.

* corresponding author's e-mail: agnieszka.ruppert@p.lodz.pl

Abstract

The establishment of the future biorefinery schemes requires the sustainable conversion and valorisation of renewable bioresources into eco-friendly fuels and chemicals. To this end, 2,5-dimethylfuran (DMF) is a promising biofuel competitive to benchmarks like ethanol due to high-value intrinsic properties. It can be produced by the catalytic hydrogenation of the 5-hydroxymethylfurfural (HMF) platform molecule, one of the biobased intermediate chemicals derived from the abundant lignocellulosic biomass. We evidenced that bimetallic NiFe alloys supported on TiO_2 are earth-abundant non-noble metal-based catalysts allowing the high yield production of DMF to be achieved. We showed that the preparation method and the reduction temperature of the catalyst are of prime importance, and are directly influencing the structure of the supported NiFe bimetallic particles and in consequence the catalyst behaviour. The

highest yield to DMF is obtained on a catalyst prepared by co-impregnation and reduced at 500°C, that features an unperfect core/shell structure of the NiFe alloy, with a partial Fe shell surrounding an Fe-enriched Ni core. The key-feature necessary for achieving high performance lies on the surface structure of the NiFe alloy that allows for an optimum availability of highly active Ni domains. The Ni atoms were maintained highly dispersed by the presence of Fe-containing surface phases. The specific surface structure is proposed to promote the HMF adsorption through the carbonyl group, while preventing from the hydrogenation of the aromatic furan ring to maintain high selectivity.

Keywords: Sustainable furanic biofuel; 2,5-dimethylfuran ; 5-hydroxymethylfurfural ; Ni-Fe/TiO_2 catalysts.

1. Introduction

Lignocellulosic biomass is an easily available and abundant valuable source of various platform molecules such as 5-hydroxymethylfurfural (HMF), the so-called “sleeping giant” of biobased intermediate chemicals [1]. HMF can be conveniently catalytically transformed by hydrogenation into a span of industrially-viable products, among which 2,5-dimethylfuran (DMF) has been given a significant attention due to its potential application as biofuel or fuel additive. Compared to known benchmarks like ethanol, DMF has higher energy density and boiling point as well as octane number. It benefits at the same time from of lower volatility and positively is not miscible with water. Consequently, selective production of DMF from HMF with high yield is of great interest [2-7].

Two competitive hydrogenation pathways of HMF to DMF are shown in Scheme 1, denoted as path A and B. Path A starts with the hydrodeoxygenation (hydroxy group removal)

of HMF that yields to 5-methylfurfural (5-MF). Subsequent reduction of carbonyl moiety produces 5-methylfurfurylalcohol (5-MFA) which in turn undergoes another hydrodeoxygenation leading to DMF as targeted product. Alternatively, 5-MFA may be dearomatized *via* furan ring hydrogenation giving 5-methyltetrahydrofuran alcohol (5-MTHFA). Both DMF and 5-MTHFA may be further hydrogenated to 2,5-dimethyltetrahydrofuran (DMTHF). In contrast, path B begins with the reduction of the aldehyde group of HMF giving 2,5-bis(hydroxymethyl)furan (BHMF). BHMF may be hydrodeoxygenated to 5-MFA and subsequently follow the same reaction pattern as described for Path A or be saturated to 2,5-bis(hydroxymethyl)tetrahydrofuran (BHMTHF) with furan ring hydrogenation. Although further hydrogenation of BHMTHF is also possible, it is not widely observed [8,9].

Considering the span of parallel and consecutive reactions, and consequently the number of possible HMF hydrogenation products, the catalyst choice is of crucial importance. As regards of the DMF production, the catalyst should be tailored with focus on the selectivity to remove both aldehyde and hydroxy groups, without saturating the aromatic ring.

Currently used systems that are often based on noble metals give undesired over-hydrogenation products like BHMTHF and DMTHF, [10,11] or even cracking reactions, e.g. with the formation of furans and the opening of furan ring [11]. These in turn may cause the catalyst deactivation due to the deposition of carbon impurities [11,12].

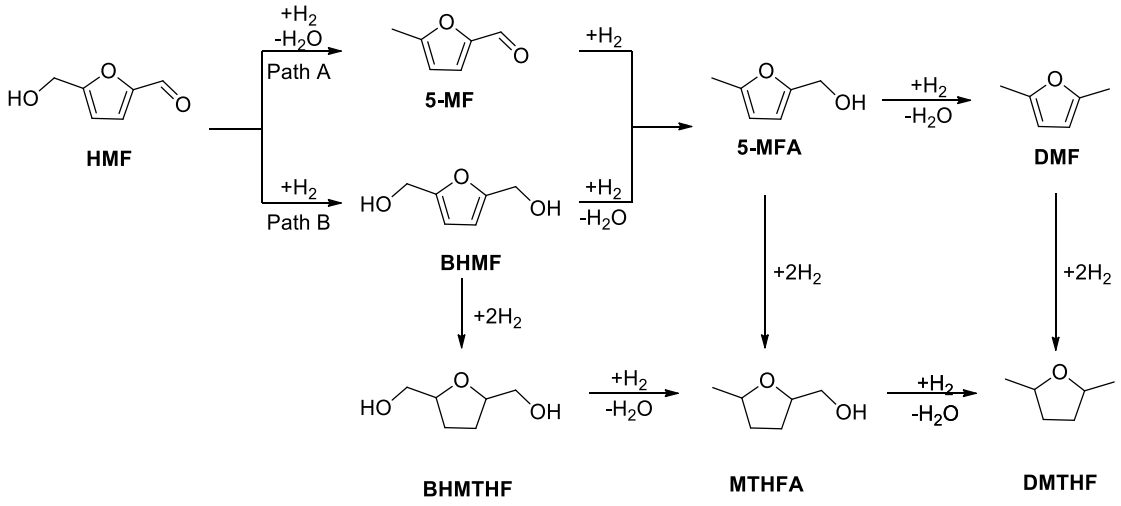

Scheme 1. Reaction pathway of HMF hydrodeoxygenation

Luo *et al.* demonstrated that carbon supported Pt, Ir, Pd and Ru catalysts can give over-hydrogenated products when processing the reaction for too-extended time, with in turn a lowering of the DMF yield. The highest DMF yield obtained for 10%Ir/C and 10%Pd/C slightly overruns 50 % [13]. Priecel *et al.* showed also the excessive activity of 5%Ru/C and 5%Ru/CNT, with a yield to the unwanted DMTHF reaching 50% and 65% after 2 h and 4 h of HMF hydrogenation, respectively [14]. Moreover it was proved that monometallic Ru favours the undesired breaking of C-C bonds instead of the hydrodeoxygenation reaction [15]. Similarly, application of Raney Ni in HMF hydrogenation at 100°C did not prevent the production of over-hydrogenated BHMTHF. Unfortunately, in this case of non-supported catalyst, possibilities to improve the selectivity and to mitigate the share of over-hydrogenation side-products are very limited [16].

The activity and selectivity of nickel-based supported catalysts strongly depend on the support properties. Metal oxides, well-known for their ability to enhance the adsorption of the C=O group of HMF on the Lewis acid sites of the catalyst, are supports of choice [17].

To address over-hydrogenation [16], decarbonylation [2,18] and ring opening [19] issues associated to monometallic catalysts, adding a second metal is a worth strategy to modulate the

catalyst properties. In contrast to the alleviation of the activity of noble metals, the use of bimetallic catalysts based on non-noble metals like Fe, Co, Ni or Cu is a more economically-reasonable approach [20]. Among them, Co is the most expensive metal, while Cu remains hard to disperse on metal oxide supports, what causes a low catalytic activity. On the other hand, Ni-based bimetallic catalysts have already been successfully employed in various hydrogenation reactions, including the transformation of HMF to DMF, and their highly-appealing activity is attributed to specific properties originating from synergistic or bifunctional effects that are not observed in their monometallic counterparts.

Indeed, Seemala et al. obtained a high yield to DMF at 200°C after 8 h of reaction over a Cu-Ni/TiO_2 catalyst. Interestingly, the formation of a core@shell-like structure by metal segregation with a Cu-enriched surface and a Ni core interacting with the TiO_2 support was pointed out as being responsible for reaching high selectivity and high catalytic performance. Likewise, Fe-containing materials were presented as promising catalysts in several hydroconversion reactions of organic molecules [21]. In particular, the much higher activity of a Ni-Fe catalyst supported on silica compared to its Ni-Cu counterpart for a similar Ni:Me ratio of 3:1 was first reported by Kumbar et al. in 1992 in the selective hydrogenation of acetophenone and benzonitrile [22]. Recently, Shi et al. indicated that heterogeneities in the structure of reduced Ni-Fe nanoparticles are key to understand the catalytic behaviour of SiO_2 supported bimetallic Ni-Fe systems in the liquid-phase hydroconversion of furfural into furfuryl alcohol [23]. However, in spite of multiple works reporting on the successful application of Ni-Fe catalysts, it must be said that barely a few works explains the role of Ni-Fe interactions on the catalytic activity of supported Ni-Fe bimetallic systems for the hydrogenation of HMF [24,25].

Yu et al. showed that even a small addition of Fe to Ni catalyst positively affected the selectivity of the HMF hydrogenation to BHMF and mitigated the formation of undesired by-

products, while the highest yield to BHMF was achieved on a 10 wt.% $Ni_{50}Fe_{50}$/CNT catalyst [25]. We recently showed also the beneficial effect of the formation of a Ni-Fe alloy for the selective cleavage of the C-O bond. We proved that the introduction of Fe to a high surface area TiO_2 supported Ni catalyst not only can improve the selectivity of the HMF hydrogenation to DMF, but also helps to improve the catalyst stability [24]. The 5:5 Ni:Fe ratio was the optimal ratio allowing the highest selectivity towards DMF to be achieved. This proof of principle study showed that further investigation remains necessary for getting better knowledge on the key-parameters driving the optimal physicochemical properties of the catalysts, and how they can tune the catalytic activity, particularly taking into account the very versatile and tunable character of Fe-Ni systems.

Therefore, our work aims at investigating to which extent the performance of TiO_2 supported Ni-Fe bimetallic catalysts in the HMF hydrogenation to DMF can be influenced by the preparation method, and notably by the temperature of the catalyst reduction. Key-factors responsible for the catalyst performances were derived and related to the main physico-chemical properties of the bimetallic Ni-Fe/TiO_2 catalysts. Particularly the structure and the alloy composition were found to determine the HMF conversion and to tune the yield to the reaction products.

2. Experimental

2.1. Materials and methods

TiO_2 support (PC500) was delivered by Millenium-Crystal (France). 5-Hydroxymethylfurfural (98%) was purchased from Fluorochem Ltd (United Kingdom) and metal precursors $Ni(NO_3)_2 \cdot 6{\cdot}H_2O$ (98%) and $Fe(NO_3)_3{\cdot}9\ H_2O$ (99 %) were supplied by Chempur (Poland). 1,4-Dioxane (99%) used as solvent was provided by Merck (Germany).

2.2. Catalyst preparation

Bimetallic catalysts based on nickel and iron were prepared with a nominal content of each metal of 5% wt. relative to the TiO_2 support, and labelled as NiFe (S1), NiFe (S2), NiFe (P) and NiFe (C).

The NiFe (S1) catalyst was prepared by a two-step wet impregnation method. First, an appropriate amount of metal precursor $Ni(NO_3)_2 \cdot 6\ H_2O$ was dissolved in distilled water. After addition of TiO_2 PC 500, the mixture was kept for 24 h. Excess of solvent was removed using rotative evaporator and the solid residue was dried at 120°C for 2 h and further calcined at 500°C for 5 h under air flow. Second, $Fe(NO_3)_3 \cdot 9H_2O$ was dissolved in distilled water and calcined NiO/TiO_2 was added and mixed. After 24 h, the solvent was removed using a rotative evaporator, the solid residue was dried at 120°C for 2 h and the catalyst was further calcined at 500°C for 5 h. Finally, the catalyst was reduced at 500°C for 1 h under H_2 flow.

The NiFe catalyst (S2) was prepared in a similar way than NiFe (S1), except that iron was deposited first.

The NiFe (P) catalyst was prepared by the precipitation method. First $Fe(NO_3)_3 \cdot 9H_2O$ was dissolved in distilled water and mixed with TiO_2 PC 500 under stirring. After dropwise addition of 5.5 mL of 25% NH_3 (aq.) at room temperature, the slurry was heat to 85°C and stirred for 24 h. The mixture was cooled down to room temperature, and the solid material was separated from the solution by filtration and washed with distilled water until neutral pH. The sample was further dried at 100°C for 24 h and calcinated at 400°C for 5 h under air flow. Next, $Ni(NO_3)_2 \cdot 6\ H_2O$ was introduced using the wet impregnation method as for other catalysts. Finally, the catalyst was reduced at 500°C for 1 h under H_2 flow directly before reaction.

The NiFe (C) catalysts were prepared by the wet co-impregnation method. Both $Fe(NO_3)_3 \cdot 9H_2O$ and $Ni(NO_3)_2 \cdot 6\ H_2O$ precursors were dissolved in distilled water and TiO_2 PC

500 was added. The mixture was kept under thorough stirring for 24 h. The water solvent was further removed using a rotative evaporator and the solid residue was dried in 120°C for 2 h. After calcination at 500°C for 5 h under air flow, the catalyst was reduced at a temperature ranging from 200°C to 600°C for 1 h under H_2 flow directly before reaction.

For comparison, Ni and Fe monometallic catalysts were prepared by a one-step wet impregnation method in a similar way than NiFe (S1) or NiFe(S2), with a final reduction temperature of 500°C.

Independently of the catalyst, the oxidation step was performed with a heating rate of 5°C/min and a 20 cm^3/min flow, while a heating rate of 15°C/min and a 50 cm^3/min flow were used for the final reduction step. In all cases, the catalysts after reduction were cooled down to room temperature under H_2 flow before being rapidly transferred to the reactor.

2.3. Characterization techniques

Inductively coupled plasma optical emission spectroscopy (ICP-OES) was carried out on an Optima 7000 DV spectrometer (Perkin Elmer), after a microwave-assisted acidic dissolution in aqua regia at 185°C under autogenic pressure. Independently on the preparation method, real Fe and Ni weight contents were measured at 5.0% ± 0.2%."

X-ray diffraction (XRD) measurements were collected using a PANalyticalX'Pert Pro MPD diffractometer. The X-ray source was a copper long fine focus X-ray diffraction tube operating at 40 kV and 30 mA. Data were collected in the 5–90° 2θ range with 0.0167° step. Crystalline phases were identified by references to the ICDD PDF-2 (version 2004) database.

Surface area and porosimetry measurements were carried out on ASAP2020 Micromeritics using N_2 as adsorbant at -196°C, with a prior outgassing under vacuum at 200°C for 3 h in order to desorb the impurities or moisture.

Temperature-programmed desorption of NH_3 (NH_3-TPD) was used to assess the acidity of the catalysts. In a typical TPD protocol, the reduced sample was placed in a quartz flow reactor and heated at 500°C under He flow for 1 h to remove impurities from the surface. Adsorption of NH_3 was carried out at 100°C for 15 min. Physically-adsorbed NH_3 molecules were removed by treating the sample with He for 15 min at 100°C before the TPD experiment was carried out from room temperature to 500°C with a 25°C min^{-1} temperature ramp (TCD detector).

Temperature-programmed reduction (TPR) was used for examining the catalyst reducibility, and performed on the AMI1 system from Altamira Instruments, USA, equipped with TCD. Before the measurements, the reduced catalysts were heated at 300°C for 30 min in a mixture of 2 vol.% O_2 and 98 vol.% Ar at a space velocity W/F = 1.11×10^{-5} g/h cm^3 (10°C/min heating rate). TPR profiles were recorded from 35°C up to 800°C, with a heating rate of 7°C/min, using a mixture of 5 vol.% H_2 and 95 vol.% Ar at a similar space velocity.

Time-of-Flight Secondary Ion Mass Spectrometry (ToF-SIMS) measurements were performed using an ION-TOF GmbH instrument (TOF-SIMS IV) equipped with a 25 kV pulsed Bi^+ primary ion gun in the static mode. The samples were fixed to the sample holder by double sided adhesive tape. The analyzed area of the sample surface was 500 μm x 500 μm. During the analysis, a pulsed low-energy electron flood gun was used for charge neutralization.

CO-adsorbed FTIR spectra were registered on a Nicolett 6700 spectrometer equipped with MCT detector and a diffuse reflection chamber. Prior to exposure to CO, the samples were reduced at an appropriate temperature in 5% H_2 in Ar for 1 h, then cooled to room temperature in an Ar flow to remove the adsorbed hydrogen and the background spectra were collected. CO adsorption was carried out for 30 min at 5 bar pressure of CO (5 vol.%) in Ar. Each spectrum was recorded with a resolution of 4 cm^{-1} performing 64 scans.

Transmission electron microscopy (TEM) mapping characterization was performed in a JEOL 2100F corrected Scanning Transmission Electron Microscope (STEM) equipped with a energy-dispersive X-ray (EDX) detector. The microscope was operated at 200 kV acceleration voltage.

2.4. Catalytic tests

The catalysts were tested in the 5-hydoxymethylfurfural (5-HMF) hydrogenation. The activity tests were performed in a 60 mL stainless-steel batch autoclave (Premex, Switzerland). The reactions were carried out with 1 g of 5-HMF, 0.15 g of catalyst and 30 mL of 1,4-dioxane. The reactor was flushed twice with hydrogen to remove air and further pressurized with hydrogen to 50 bar at room temperature. The reaction was performed at 220°C for 1 h with a stirring rate of 650 rpm. Afterwards, the reactor was cooled down to room temperature and the reaction mixture was centrifuged for 5 min at 3500 rpm to separate the catalysts from the liquid sample.

Reaction products were analysed using a GC instrument (Agilent 7820 A) equipped with a FID detector and high polarity wax column Agilent J&W CP-Wax 52 CB. Essential parameters were the following: injection volume 1.0 μL, inlet temperature 300°C, detector temperature 300°C, split flow 163.69 mL/min, column flow 1.6369 mL/min (N_2). The initial column temperature was 50°C (5 min) with a temperature rise of 12°C/min and a final temperature of 200°C (20 min). The concentration of each compound in the product mixture was determined using calibration curves of pure compounds solution.

The activity of the catalysts were expressed in terms of HMF conversion and of reaction yields to given products, calculated as follows:

$$Conversion = \frac{n_{HMF_i} - n_{HMF_r}}{n_{HMF_i}} \cdot 100\%$$

$$Yield_p = \frac{n_p}{n_{HMF_i}} \cdot 100\%$$

where $n(HMF)_i$ and $n(HMF)_r$ are the number of moles of HMF molecules, before and after test, respectively, and n(p) is the number of moles of a given product within the reaction mixture.

3. Results

3.1. Characterization of the TiO_2 supported mono and NiFe bimetallic catalysts

The XRD patterns of the bimetallic nickel-iron catalysts are shown in Figure 1 and their main physico-chemical properties are listed in Table 1. The characteristic signature of the TiO_2 anatase support was observed, and all the support reflexes were indexed in the *I*41/*amd* tetragonal unit cell of the anatase TiO_2 polymorph, notably at 2θ = 25.3°, 37.8°, 48.1°, 53.9°, 55.1°, 62.7°, 68.8°, 70.3°, 75.0°. No peaks suggesting the presence of metallic or oxide phases of iron or nickel were detected. By contrast, the diffraction peaks observed within the regions 43–44° and 50–51° in 2θ were assigned respectively to the (111) and (200) reflections of Ni-rich Ni-Fe solid solution (NiFe alloy) with face-centered-cubic (fcc) structure (JCPDS card no. 38-0419) [26-28]. It should be noted that the body-centred cubic (bcc) phase of the NiFe alloy was not observed in our conditions, in agreement with Wojcieszak et al. on $NiFe/SiO_2$ systems [23]. In NiFe alloys, the bcc phase is usually reported to be stable with small Ni concentrations [29].

The low-angle shift observed in comparison to the characteristic 2θ value of metallic Ni (111) (2θ = 44.4° – JCPDS 04-0850) is also reported to evidence the formation of the Ni-rich NiFe alloy [30]. The structure of the NiFe alloy strongly depends on both Fe and Ni contents,

that are determining the extent of the shift of the reflex position. The peak assigned to the NiFe alloy in the 43–44° region is gradually shifted towards lower angles with the increase in the catalyst reduction temperature from 300°C to 600°C, the shift at 2θ = 43.8° being maximum after reduction at 600°C. This is related to the dynamic change of the alloy composition. The diffusion of iron atoms into the host nickel crystallites causes an increase in the lattice parameters due to the larger radius of Fe in comparison to Ni. [31-33]. Thus, the shift of the NiFe alloy peak towards lower angles suggested an enrichment of the alloy composition with Fe. This enrichment in iron of the NiFe alloy was accompanied by a slight increase in the crystallite size from 9 nm at 300°C to 15 nm at 600°C.

When it comes to the catalysts prepared using different methods, the peak assigned to the Ni-rich NiFe alloy is also visible at 43.8° for both NiFe(S1) and NiFe(S2) catalysts with a similar average crystallite size. A slight shift towards higher 2θ angles is noticeable for the NiFe(P) catalyst, which suggests a lower Fe enrichment in comparison to other bimetallic samples.

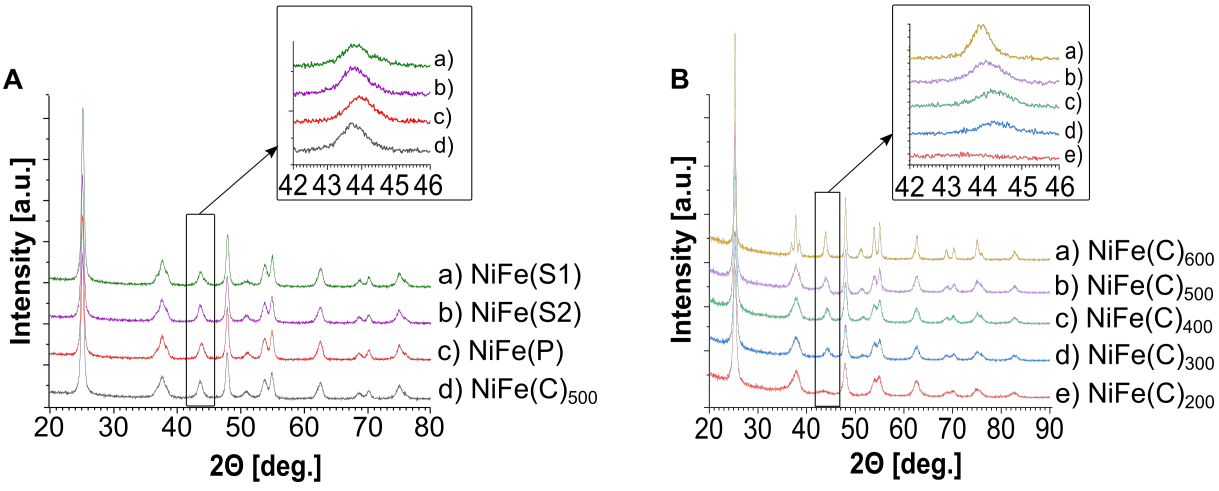

Figure 1. Powder XRD patterns of TiO_2 supported NiFe bimetallic catalysts, **(A)** influence of the preparation method with final reduction at 500°C, **(B)** influence of the reduction temperature for the NiFe(C) catalyst.

In comparison to the bare un-treated TiO_2 support with a specific surface area of 322 m^2/g, the NiFe bimetallic supported catalysts display lower surface areas of about 110 m^2/g, 80 m^2/g and 13 m^2/g for a reduction temperature of 200-400°C, 500°C and 600°C, independently of the preparation method. For the TiO_2 PC500 support with a mean crystallite size of 7 nm, it is known that the specific surface area and the pore volume of the catalysts are directly related to the mean size of the TiO_2 crystallites, that is increasing with the increase in the temperature of the thermal treatments. This was visualized by the gradual sharpening of the main diffraction peak of the anatase phase of the TiO_2 support, that corresponded to an increase in the mean anatase crystallite size up to 14 nm and 24 nm at 500°C and 600°C, respectively. This was associated to a decrease in the pore volume too.

< Table 1 >

Table 1. Physicochemical properties of the NiFe bimetallic catalysts.

Catalyst	BET Surface area [m^2/g]	Total pore volume [cm^3/g]	NiFe alloy mean cristallite size [nm]	Anatase TiO_2 mean crystallite size [nm] [a]	Acidity [μmol/g]
TiO_2	322	0.46	-	7	-
Ni	-	-	-	-	130
Fe	-	-	-	-	180
NiFe (S1)	80	0.26	10	14	670
NiFe (S2)	78	0.26	10	14	475
NiFe (P)	81	0.31	14	14	530
NiFe (C)-200	110	0.34	-	11	739
NiFe (C)-300	108	0.36	9	12	553
NiFe (C)-400	109	0.35	11	12	460
NiFe (C)-500	81	0.26	12	14	590
NiFe (C)-600	13	0.14	15	24	220

[a] The mean crystallite size for TiO_2 defined as the average size of the coherently diffracting domains, was determined by applying the Scherrer equation to the (101) peak of anatase at 25.7°, with the usual assumption of spherical crystallites taking into account the intrinsic broadening of the peaks due to the instrumentation.

NH_3-TPD was used to determine the acidity of the catalysts, summarized in Table 1. The acidity of both monometallic catalysts stays in the same range with a slightly higher acidity for the Fe catalyst, that can be explained by its stronger oxyphilic character and affinity to the O-atom [21,34]. The interaction between Fe and O atoms of support can lead to a partial positive charging of the Fe atoms that in turn favour NH_3 adsorption and enhances the surface acidity [35]. As regards of the monometallic counterparts, the strongly higher acidity of bimetallic NiFe catalysts reveals the key-role played by the NiFe alloy in interaction with the TiO_2 support, that creates additional (novel) metallic surface sites acting as centers for NH_3 adsorption. However, the results showed that the acidity of the bimetallic catalysts reduced at 500°C depends on its synthesis method, the lowest and the highest acidity being obtained for the NiFe (S2) and NiFe (S1) catalysts, at 475 μmol/g and 670 μmol/g, respectively.

The number of acidic centers on the surface of the bimetallic NiFe catalysts depends also on its reduction temperature. The highest acidity was observed for the catalyst NiFe (C) reduced at the low temperature of 200°C. This could be explained by the residual presence of metal oxides on the catalyst surface, that are known to act as additional Lewis acid sites next to the acid sites of titania [36,37]. The acidity of the surface decreases with increasing the reduction temperature to 400°C due to the gradual reduction of nickel and iron oxides into metallic phases. The acidity of the catalyst reduced at 500°C was slightly higher – 590 μmol/g. The significantly lower acidity of the catalyst reduced at 600°C is caused probably by the decrease of the surface area of the support and the increased size of the metal particles.

The reducibility of the NiFe catalysts prepared using different methods was studied by TPR measurements. Figure 2 shows the reduction profiles recorded on the bimetallic catalysts as well as on their monometallic counterparts. They are characterized by the presence of a single reduction peak for all investigated catalysts, that however differs in terms of temperature range

(peak width) and maximum. The reduction of the monometallic Ni catalyst takes place in one step with a maximum of hydrogen consumption at *ca.* 425°C that indicates a relatively strong interaction between the metal and the support surface [38,39]. By contrast, monometallic Fe catalyst displays a single reduction peak with a maximum around 340°C assigned to the two-step iron oxides reduction, as typically observed for low-loaded iron catalysts [40]. As far as the bimetallic Ni-Fe catalysts were concerned, the reduction profiles displayed a main peak ranging from 300°C to 500°C attributed to the reduction of oxide phases of both metals. They evidenced a shift towards lower temperatures of the maximum of hydrogen consumption, at 415°C, 405°C, 385°C and 390°C for NiFe (S1), NiFe (S2), NiFe (P) and NiFe (C)-500 catalysts, respectively. This suggests that, whatever the preparation methods, both metal species are in close contact which affects their reducibility [25]. In an interdependent manner, the presence of Fe can induce the reduction of nickel oxide, while the presence of Ni can inhibit the reduction of iron oxide [41]. Moreover, the diffusion of Fe atoms into the Ni crystallites during the formation of the alloy structure is proposed to weaken the interaction of the host metal with the support, what in turn may also facilitate the reducibility of Ni species. It must be noted that among all bimetallic catalysts, the sharpest reduction peak in a narrow temperature range was observed for the Ni-Fe(C)-500 sample. This might evidence the strongest synergy between both metals during the reduction of the oxides, able to impact in an homogeneous way on the reduction temperature of both species.

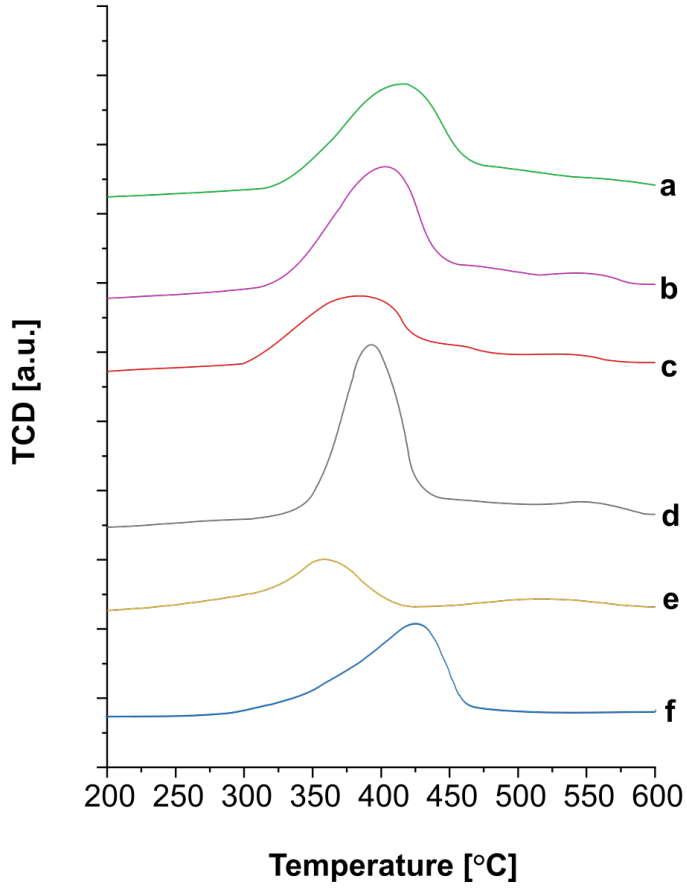

350

351

352 **Figure 2.** TPR profiles of the TiO_2 supported mono and bimetallic catalysts: a) NiFe (S1); b)
353 NiFe (S2), c) NiFe (P), d) NiFe(C)-500, e) Fe and f) Ni.

354

355 FTIR spectra of CO adsorbed on the NiFe bimetallic catalysts were recorded to characterize
356 the effect of both the reduction temperature and the preparation method on the qualitative and
357 quantitative change of adsorption sites on the surface of the bimetallic catalysts (Figure 3).
358 Under given conditions, it must be noted that CO does not adsorb at the surface of Fe species,
359 so that all the bands are attributed to CO adsorbed on nickel species [24].

360 Typically, in the 2000-2100 cm^{-1} range, the bands reflect the linear adsorption of CO on
361 metallic nickel crystallites. In particular, the bands at 2084 cm^{-1}, 2056 cm^{-1} and 2025 cm^{-1} are

assigned to CO linearly-adsorbed on highly dispersed metal crystallites, to physically-adsorbed CO and to the linear adsorption of CO on moderately-dispersed metal, respectively [42,43].

First it is worth noting that both parameters investigated did not significantly influence the nature of the surface sites, as similar bands were observed (*eg.* no appearance of lower-wavenumber bands assigned to bridged CO adsorption, no shift in wavenumbers). Fig. 3A shows that the preparation method has an important effect on the availability of Ni at the surface of the bimetallic NiFe catalysts. Indeed, in terms of band intensity, the following ranking was observed: NiFe (S1) > NiFe (C)-500 and NiFe (S2) > NiFe(P). In particular the availability of Ni for the catalysts prepared by successive impregnation is related to the impregnation sequence, as Ni was introduced last in the case of the NiFe (S1) catalyst, and first for the NiFe (S2) counterpart.

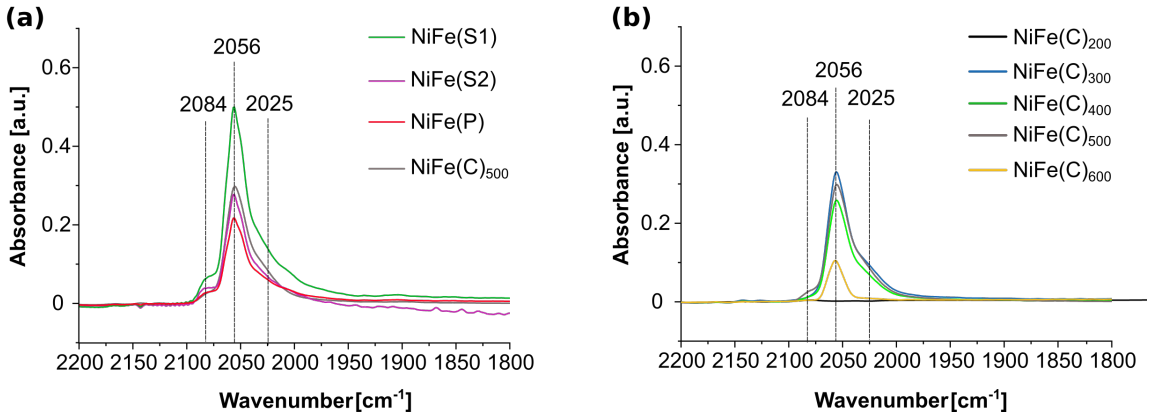

Figure 3. CO-adsorbed FTIR spectra of TiO_2 supported NiFe bimetallic catalysts. **(a)** influence of the preparation method, **(b)** influence of the reduction temperature for NiFe (C) catalysts

The reduction temperature had also a significant influence on the surface availability of Ni species. The spectra recorded on the catalyst submitted to a thermal treatment at 200°C did not show any bands, probably due to the presence of the metal oxides, which limits the adsorption

of the probe molecule. After reduction within the 300-500°C range, relatively similar band intensities were observed indicating an approximatively identical availability of the Ni metallic sites. Increasing further the reduction temperature to 600°C caused a decrease in the band intensity, which indicates a lowering of the number of Ni surface sites available for the CO adsorption.

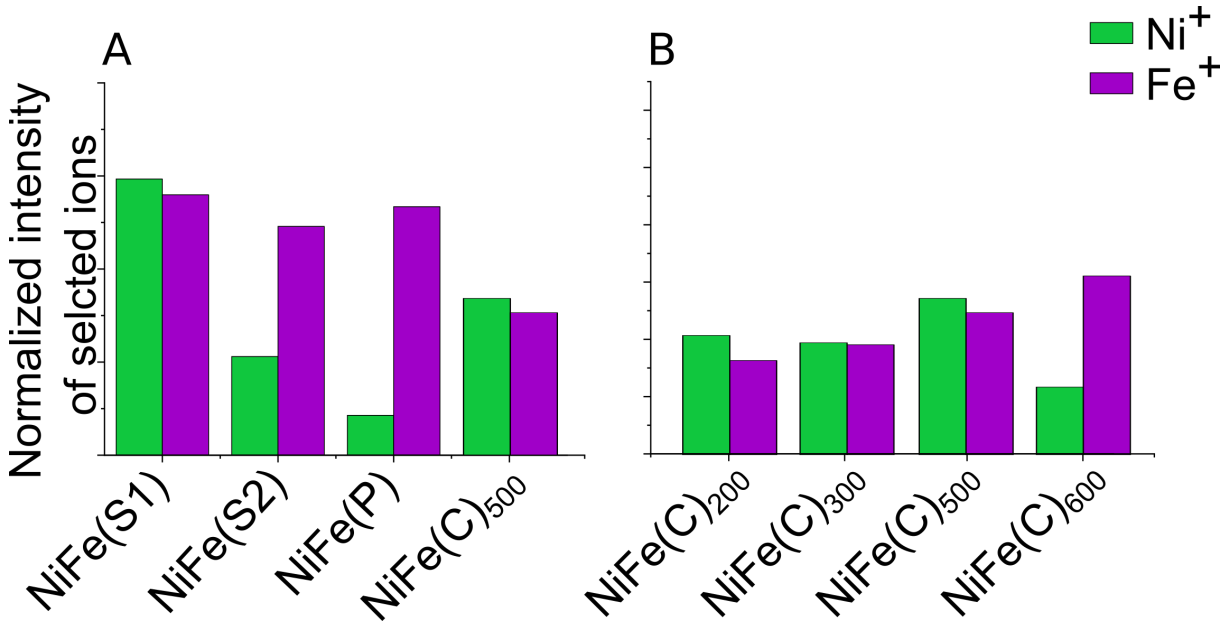

Figure 4. Normalized intensity of selected ions calculated on the basis of ToF-SIMS spectra collected from the surface of TiO_2 supported bimetallic NiFe catalysts, **(A)** influence of the preparation method with a reduction temperature of 500°C, **(B)** influence of the reduction temperature for NiFe (C) catalysts.

The influence of both the preparation method and the reduction temperature on the normalized intensity of selected ions identified on the catalyst surface is shown in Fig. 4. Interestingly a similar normalized intensity was recorded for Ni^+ and Fe^+ in the case of NiFe(S1) and NiFe (C)-500 catalysts in contrast to both NiFe(S2) and NiFe(P) catalysts for which Fe was

predominantly exposed on the surface in comparison to Ni, in a larger extent in the case of the NiFe(P) catalyst. The reduction temperature had as well a prime importance on the relative presence of Ni and Fe species at the surface. Here, considering the accuracy of the measurements, it can be noted that in the 200-500°C temperature range, similar Ni^{+}/Fe^{+} ratios were observed, while increasing the reduction temperature to 600°C led to a drastic change of the surface composition, with a pronounced increase in the Fe presence at the catalyst surface.

3.2. Catalytic activity

Table 2 shows the activity of the bimetallic NiFe catalysts in the HMF hydrodeoxygenation, expressed in terms of HMF conversion and yields to the different products. Regardless of the preparation method, a high conversion of the HMF substrate (over 94 %) was obtained with each catalyst, and almost no ring hydrogenation products (BHMTHF, MTHFA, DMTHF) were observed. By contrast, the catalysts strongly differentiate in terms of distribution of the reaction products. The highest yield towards DMF was obtained on NiFe (C)-500 and NiFe (S1) catalysts, at 71% and 61%, respectively. Both NiFe(S2) and NiFe (P) catalysts displayed far lower DMF yields of 23% and 20%, respectively, with a more homogeneous distribution towards the main products observed, namely 5-MFA, BHMF and DMF.

< Table 2 >

423 **Table 2. Influence of the preparation method on the activity of the NiFe catalysts reduced at 500°C.**

Catalysts	HMF conversion [%]	Product yield [%]							
		5-MF	BHMF	BHMTHF	5-MFA	DMF	MTHFA	DMTHF	OTHERS
NiFe (S1)	100	1	8	1	20	61	0	0	8
NiFe (S2)	94	6	27	0	27	23	0	0	10
NiFe (P)	100	6	28	2	40	20	0	0	5
NiFe (C)-500	96	10	2	0	6	71	0	0	7

424 Reaction conditions: 220°C; 1 h; 0.15 g of catalyst; 1 g of HMF; 30 ml of dioxane; 30 bar of hydrogen
425

426

427 **Table 3. Influence of the reduction temperature on the activity of the NiFe(C) catalysts**

Temperature of reduction [°C]	HMF Conversion [%]	Product yield [%]							
		5-MF	BHMF	BHMTHF	5-MFA	DMF	MTHFA	DMTHF	OTHERS
200	11	3	1	0	0	0	0	0	7
300	100	3	3	0	20	69	0	0	5
400	100	0	3	0	24	69	0	0	4
500	96	10	2	0	6	71	0	0	7
600	42	14	8	0	13	5	0	0	3

428 Reaction conditions: 220°C; 1 h; 0.15 g of catalyst; 1 g of HMF; 30 ml of dioxane; 30 bar of hydrogen

Next, the influence of the reduction temperature of the NiFe(C) prepared by the wet co-impregnation method on the catalyst activity is shown in Table 3. The catalyst treated at the temperature of 200°C showed a very low activity, with a HMF conversion of 11% and no DMF formation. This could be explained by the residual presence of metal oxides on the catalyst surface. A significant increase in activity was observed after reduction of the catalyst within the 300-500°C temperature range. Reactions with the catalysts reduced at 300°C and 400°C allowed complete HMF substrate conversion to be achieved, together with a similar DMF yield of 69%. The highest performance was shown by the catalyst reduced at 500°C, namely a nearly-full HMF conversion of 96%, and the highest DMF yield of 71%. By contrast, reducing the catalyst at the higher temperature of 600°C caused a drastic decrease in the activity of the catalyst, with a low HMF conversion of 42%, and a very low DMF yield of 5%.

< Table 3 >

4. Discussion

The activity of the TiO_2 supported NiFe bimetallic catalysts in the hydrogenation of HMF into DMF was investigated, and several key factors with significant influence on the reaction have been identified by studying the influence of both the preparation method and the reduction temperature. The results showed that the structure of the NiFe bimetallic particles strongly impacted the catalytic behaviour. To this end, additional TEM analysis with EDX elementary mapping and line scan profile has been conducted on both NiFe(C)-500 and NiFe(C)-600 catalysts, as they displayed respectively the highest and the lowest DMF yield among the series of catalysts (Figure 5).

First, the catalysts cannot be considered *sensu stricto* as supported catalysts, with dispersed metallic nanoparticles supported on a TiO_2 host, due to similar particle sizes between the anatase crystallites and the metallic phase. In-depth characterization of these systems is challenging, as they are known to show a poor Z-contrast, that prevents from a doubtless identification of phases by TEM imaging [23]. However, as regards of the NiFe(C)-500 catalyst, the EDX mapping and the line scan profile confirmed the formation of NiFe alloy structures with a core/shell structure (Fig. 5a-e), with a Ni-rich core, and a majority of Fe as Fe-rich phases or nanoparticles composing the shell. In agreement with recent reference works on bimetallic systems [44,45], larger red areas in comparison to green ones (Fig. 5a vs. 5b) , and the typical EDX line profile with only Fe visible at both sides (Fig. 5e), were observed. The partial (non-perfect) nature of the core-shell structure is suggested as red areas corresponding to Ni atoms remain visible on the overlay image (Fig. 5c). This is in good agreement with both CO adsorbed-FTIR and ToF-SIMS analyses that showed the clear availability of Ni species at the surface of the NiFe alloy.

By contrast, the higher reduction temperature of 600°C caused a redispersion and homogenisation of the Fe atoms within the NiFe alloy, as no core-shell structure was evidenced on the EDX mapping and the line scan profile (Fig. 5f-j). The temperature probably allowed surface diffusion of the Fe atoms of Fe-rich shell, in agreement with the lower availability of Ni species evidenced by CO adsorbed-FTIR and ToF-SIMS. It also allowed enhanced diffusion to the bulk of the alloy, in agreement with the Fe-enrichment of the Ni core observed by XRD.

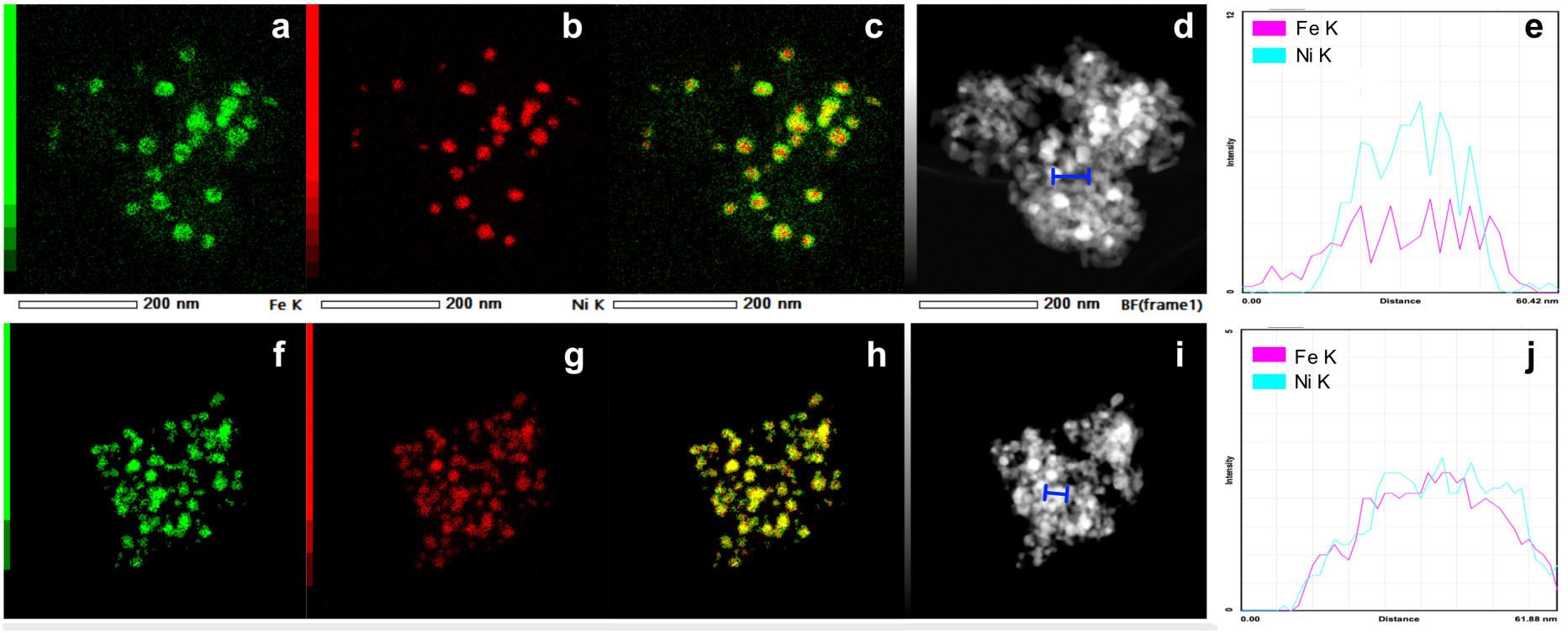

Figure 5. EDX elementary mapping and line scan profile for the NiFe(C) catalysts reduced at 500°C **(top, a-e)** and 600°C **(bottom, f-j)**. **(a,f)** Fe-K EDX map of (d,i), **(b,g)** Ni-K EDX map of (d,i), **(c,h)** overlay image of (a,f) and (b,g), **(d,i)** Bright field image in STEM mode, **(e,j)** EDX line profiles across the nanoparticles along the blue line shown in the images (d,i).

Our earlier works showed that the formation of a NiFe alloy influences both activity and selectivity in the HMF hydrogenation over bimetallic Ni-Fe catalysts [22]. In the present work, we are depicting further that the structure of the NiFe alloy is of prime importance, in particular the surface availability of Fe and Ni species, and impacts the behaviour of the catalyst.

We suggest that the discrepancy between the bulk and the surface composition of the NiFe alloy is a key-feature driving the catalytic performances. Indeed, the core/shell structure of the alloy was identified as a Fe-containing Ni-rich phase with fcc structure [46]. The higher diffusion coefficient for Fe in comparison to Ni allows the incorporation of Fe into the bulk structure of Ni. Dynamic changes of the alloy composition were observed especially with the increase of the reduction temperature of the catalysts where more Fe atoms were incorporated into the bulk structure [31]. However, it should be mentioned that the Fe-enriched core remained Ni-rich, and the bcc phase of the NiFe alloy that is characteristic of the Fe-rich alloy was not observed in our case.

The composition of the surface of the NiFe alloy differs strongly from its bulk one, and in particular with a drastic change observed between samples reduced at 500°C and 600°C. The partial or unperfect nature of the Fe shell surrounding the Fe-enriched Ni core observed at 500°C for the most efficient catalyst can be seen as a Fe-rich surface phase or as Fe nanoparticles decorating the Ni-rich core. In both cases, this surface structure and composition allow for the availability of Ni species at the catalyst surface, as evidenced by both CO adsorbed-FTIR and ToF-SIMS analyses. Similar observation was pointed out by Wojcieszak at al. where asymmetrical Fe-rich shell was developed around Ni particles in the case of Ni:Fe/SiO_2 catalysts [23].

By contrast, the absence of real core/shell structure at 600°C resulted simultaneously from the Fe-enrichment of the core and from the migration/redispersion of Fe surface species. The

redistribution of surface Fe caused a drastic lowering of the availability of surface Ni species, as visualized by the lower adsorption of CO by FTIR and the strong increase in the Fe:Ni surface ratio in the top-surface layer by ToF-SIMS. This higher Fe:Ni ratio is also observed for NiFe(S2) and NiFe(P) prepared by other methods samples and reduced at 500°C. In those three cases, the high Fe:Ni surface ratio with low Ni accessibility/availability also evidenced by FTIR was associated to low DMF yields (23%, 20% and 5% for NiFe(S2), NiFe(P) and NiFe(C)-600 catalysts, respectively) in comparison to the NiFe(C)-500 catalyst.

The lowering of the Fe:Ni ratio can also be related to the way hydrogen is chemisorbed. Indeed, hydrogen chemisorption occurs preferentially on Ni rather than on Fe [47], what provides in consequence much stronger SMSI effect on Ni. This might result in the migration of titania on Ni, and the consequent reduction of the accessibility of Ni. In particular, that effect could be pronounced at the high temperature of 600°C, for which the SMSI effect is stronger, as well as for both FeNi(S2) and FeNi(P) catalysts, for which Ni was introduced in the last step.

Ni is known to be very active in the hydrogenation of HMF, but however not very selective [8,23]. The positive impact of Fe addition may be explained by the change of HMF adsorption geometry on the NiFe bimetallic system compared to the monometallic Ni catalyst. We propose that the adsorption of HMF occurs on monometallic Ni through both furan ring and carbonyl groups, and on the NiFe alloy only through the carbonyl group, thus disfavouring the hydrogenation of the aromatic ring that would lower strongly the selectivity to DMF. This was recently suggested by Chen et al. in the case of the hydrogenation of furfural [48]. In that case, the Ni atoms are responsible for the hydrogenation and the Fe atoms are beneficial for the repulsion of the furan ring. In consequence, achieving high selectivity to DMF with a high HMF conversion on Ni-Fe catalysts would require the presence of metallic Ni sites available at the surface and maintained dispersed thanks to Fe-containing surface phases, that favour the creation of Ni-Fe interfaces and prevent from the hydrogenation of the ring.

5. Conclusions

We demonstrated the ability of earth-abundant non-noble bimetallic NiFe alloy supported on TiO_2 to be active and selective catalysts for the high yield production of 2,5-dimethylfuran from the biomass-derived 5-hydroxymethylfurfural platform molecule, as a green biofuel competitive to benchmarks like ethanol. Using TiO_2 PC500 as host support, we studied the influence of both the preparation method and the reduction temperature on the catalyst performances, and we showed that they both strongly impacted the catalyst behaviour and in turn the yield to DMF. Dynamic changes of the alloy properties were observed especially with the increase of the reduction temperature of the catalysts where more Fe atoms were incorporated into the bulk structure.

The catalyst performance is directly influenced by the structure of the NiFe alloy, with a key-feature relying on the discrepancy between its bulk and surface composition. Among the series of catalysts studied, the catalyst prepared by co-impregnation of both metal precursors and reduced at 500°C led to the highest yield to DMF of 71%, with a nearly full HMF conversion of 96%. It features a core/shell structure with an Fe-containing Ni-rich core surrounded/decorated by a partial/unperfect Fe-rich shell. This surface structure and composition allow for the availability of highly active Ni domains at the alloy surface, maintained dispersed by the exposure of Fe-rich surface phases, and is proposed to promote the HMF adsorption through the carbonyl group, while preventing from the further hydrogenation of the aromatic furan ring to maintain high selectivity. By contrast, the availability of surface Ni species is strongly lowered by the migration/redispersion of Fe surface species and the resulting loss of the core/shell structure when the catalyst is reduced at a too high temperature, what in turn leads to lower HMF conversion.

Declaration of Competing Interest

The authors declare that they have no known competing financial interests or personal relationships that could have appeared to influence the work reported in this paper.

Acknowledgements

The authors gratefully acknowledge that this work was financially supported by a grant from the National Center of Science (NCN) in Krakow OPUS-LAP (2020/39/I/ST4/02039). D. Ihiawakrim (IPCMS) is thanked for performing TEM characterizations.

References

[1] Xu H, Li X, Hu W, Lu L, Chen J, Zhu Y, et al. Recent advances on solid acid catalyic systems for production of 5-Hydroxymethylfurfural from biomass derivatives. Fuel Process Technol 2022;234:107338.

[2] Mäki-Arvela P, Ruiz D, Murzin DY. Catalytic Hydrogenation/Hydrogenolysis of 5-Hydroxymethylfurfural to 2,5-Dimethylfuran. ChemSusChem 2021;14:150–68.

[3] Le HS, Said Z, Pham MT, Le TH, Veza I, Nguyen VN, et al. Production of HMF and DMF biofuel from carbohydrates through catalytic pathways as a sustainable strategy for the future energy sector. Fuel 2022;324:124474.

[4] Esteves LM, Brijaldo MH, Oliveira EG, Martinez JJ, Rojas H, Caytuero A, et al. Effect of support on selective 5-hydroxymethylfurfural hydrogenation towards 2,5-dimethylfuran over copńper catalysts. Fuel 2020;270:117524.

[5] Wang X, Zhang C, Zhang Z, Li Q. Tuning dual active sites of Cu/CoCeOx catalysts for efficient catalytic transfer hydrogenation of 5-hydroxymethylfurfural to biofuel 2,5-dimethylfuran. Fuel 2022;320:123996.

[6] Guo D, Liu X, Cheng F, Zhao W, Wen S, Xiang Y, et al. Selective hydrogenolysis of 5-hydroxymethylfurfural to produce biofuel 2, 5-dimethylfuran over Ni/ZSM-5 catalysts. Fuel 2020;274:117853.

[7] Wang X, Liang X, Li J, Li Q. Catalytic hydrogenolysis of biomass-derived 5-hydroxymethylfurfural to biofuel 2, 5-dimethylfuran. Appl. Catal. A: Gen. 2019;576:85-95.

[8] Przydacz M, Jędrzejczyk M, Brzezińska M, Rogowski J, Keller N, Ruppert AM.

Solvothermal hydrodeoxygenation of hydroxymethylfurfural derived from biomass towards added value chemicals on Ni/TiO2 catalysts. J Supercrit Fluids 2020;163.

[9] Brzezińska M, Keller N, Ruppert AM. Self-tuned properties of CuZnO catalysts for hydroxymethylfurfural hydrodeoxygenation towards dimethylfuran production. Catal Sci Technol 2020;10:658–70.

[10] Fulignati S, Antonetti C, Licursi D, Pieraccioni M, Wilbers E, Heeres HJ, et al. Insight into the hydrogenation of pure and crude HMF to furan diols using Ru/C as catalyst. Appl Catal A Gen 2019;578:122–33.

[11] Luo J, Lee JD, Yun H, Wang C, Monai M, Murray CB, et al. Base metal-Pt alloys: A general route to high selectivity and stability in the production of biofuels from HMF. Appl Catal B Environ 2016;199:439–46.

[12] Requies JM, Frias M, Cuezva M, Iriondo A, Agirre I, Viar N. Hydrogenolysis of 5-Hydroxymethylfurfural To Produce 2,5-Dimethylfuran over ZrO2 Supported Cu and RuCu Catalysts. Ind Eng Chem Res 2018;57:11535–46.

[13] Luo J, Arroyo-Ramírez L, Wei J, Yun H, Murray CB, Gorte RJ. Comparison of HMF hydrodeoxygenation over different metal catalysts in a continuous flow reactor. Appl Catal A Gen 2015;508:86–93.

[14] Priecel P, Endot NA, Carà PD, Lopez-Sanchez JA. Fast Catalytic Hydrogenation of 2,5-Hydroxymethylfurfural to 2,5-Dimethylfuran with Ruthenium on Carbon Nanotubes. Ind Eng Chem Res 2018;57:1991–2002.

[15] Tan Q, Wang G, Nie L, Dinse A, Buda C, Shabaker J, et al. Different Product Distributions and Mechanistic Aspects of the Hydrodeoxygenation of m-Cresol over Platinum and Ruthenium Catalysts. ACS Catal 2015;5:6271–83.

[16] Kong X, Zhu Y, Zheng H, Dong F, Zhu Y, Li YW. Switchable synthesis of 2,5-dimethylfuran and 2,5-dihydroxymethyltetrahydrofuran from 5-hydroxymethylfurfural over Raney Ni catalyst. RSC Adv 2014;4:60467–72.

[17] Chimentão RJ, Oliva H, Belmar J, Morales K, Mäki-Arvela P, Wärnå J, et al. Selective hydrodeoxygenation of biomass derived 5-hydroxymethylfurfural over silica supported iridium catalysts. Appl Catal B Environ 2019;241:270–83.

[18] Duarte DP, Martínez R, Hoyos LJ. Hydrodeoxygenation of 5-Hydroxymethylfurfural over Alumina-Supported Catalysts in Aqueous Medium. Ind Eng Chem Res 2016;55:54–63.

[19] Zhu C, Liu Q, Li D, Wang H, Zhang C, Cui C, et al. Selective Hydrodeoxygenation of 5-Hydroxymethylfurfural to 2,5-Dimethylfuran over Ni Supported on Zirconium Phosphate Catalysts. ACS Omega 2018;3:7407–17.

[20] Wang X, Zhang C, Zhang Z, Gai Y, Li Q. Insights into the interfacial effects in Cu-Co/CeOx catalysts on hydrogenolysis of 5-hydroxymethylfurfural to biofuel 2,5-dimethylfuran. J. Colloid Interface Sci. 2022;615:19-29.

[21] Shi D, Wojcieszak R, Paul S, Marceau E. Ni promotion by Fe: What benefits for

627 catalytic hydrogenation? Catalysts 2019;9.

628 [22] Kumbhar PS, Kharkar MR, Yadav GD, Rajadhyaksha RA. Geometric and electronic
629 effects in silica supported bimetallic nickel-copper and nickel-iron catalysts for liquid-
630 phase hydrogenation of acetophenone and benzonitrile. J Chem Soc Chem Commun
631 1992:584–6.

632 [23] Shi D., Sadier A, Girardon J-S, Mamede A-S, Ciotonea C, Marinova M, Stievano L.,
633 Sougrati M. T., La Fontaine C., Paul S, Wojcieszak R., Marceau E. Probing the core
634 and surface composition of nanoalloy to rationalize its selectivity: Study of Ni-Fe/SiO2
635 catalysts for liquid-phase hydrogenation, Chem Catalysis 2022, 2, 7, 1686-1708.

636 [24] Przydacz M, Jędrzejczyk M, Rogowski J, Szynkowska-Jóźwik M, Ruppert AM. Highly
637 Efficient Production of DMF from Biomass-Derived HMF on Recyclable. Energies
638 2020;13:4660.

639 [25] Yu L, He L, Chen J, Zheng J, Ye L, Lin H, et al. Robust and recyclable nonprecious
640 bimetallic nanoparticles on carbon nanotubes for the hydrogenation and hydrogenolysis
641 of 5-hydroxymethylfurfural. ChemCatChem 2015;7:1701–7.

642 [26] Lu X, Huo G, Liu X, Liang G, Han Z, Song X. Hierarchical FeNi3 assemblies with
643 caltrop-like architectures: Synthesis, formation mechanism and magnetic properties.
644 CrystEngComm 2012;14:5622–6.

645 [27] Yu X, Pan Z, Zhao Z, Zhou Y, Pei C, Ma Y, et al. Boosting the Oxygen Evolution
646 Reaction by Controllably Constructing FeNi3/C Nanorods. Nanomaterials 2022;12.

647 [28] Zheng Y, Wu M, Qian C, Jin Y, Xiao W, Liang X. Tunable Electromagnetic and
648 Microwave Absorption Properties of Magnetic FeNi3 Alloys. Nanomaterials 2023;13.

649 [29] Niu ZW, Cai LC. Ab initio phase stability of some cubic phases of ordered Ni-Fe
650 alloys at high temperatures and pressures. Comput Mater Sci 2016;125:100–4.

651 [30] Putro WS, Kojima T, Hara T, Ichikuni N, Shimazu S. Selective hydrogenation of
652 unsaturated carbonyls by Ni-Fe-based alloy catalysts. Catal Sci Technol 2017;7:3637–
653 46.

654 [31] Hajalilou A, Kianvash A, Lavvafi H, Shameli K. Nanostructured soft magnetic
655 materials synthesized via mechanical alloying: a review. J Mater Sci Mater Electron
656 2018;29:1690–717.

657 [32] Ebrahimi F, Li HQ. Structure and properties of electrodeposited nanocrystalline FCC
658 Ni-Fe alloys. Rev Adv Mater Sci 2003;5:134–8.

659 [33] Mu A, Scheu C, Pokharel A, Bo S, Bein T, Fattakhova-rohlfing D. Iron-Doped Nickel
660 Oxide Nanocrystals Alkaline Water Splitting. ACS Nano 2015;9:5180–8.

661 [34] Han Q, Rehman MU, Wang J, Rykov A, Gutiérrez OY, Zhao Y, et al. The synergistic
662 effect between Ni sites and Ni-Fe alloy sites on hydrodeoxygenation of lignin-derived
663 phenols. Appl Catal B Environ 2019;253:348–58.

664 [35] Yi Y, Wang L, Guo Y, Sun S, Guo H. Plasma-assisted ammonia decomposition over

Fe–Ni alloy catalysts for COx-Free hydrogen. AIChE J 2019;65:691–701.

[36] Belokopytov V, Kholyavenko KM, Gerei S V. An infrared study of the Surface Properties of Metal Oxides 2. The Interaction of Ammonia with the Surface of Fe2O3, ZnO, MoO3, and V2O5. J Catal 1979;7:1–7.

[37] Auroux A, Gervasini H. Microcalorimetric study of the acidity and basicity of metal oxide surfaces. J Phys Chem 1990;94:6371–9.

[38] Liu J, Li C, Wang F, He S, Chen H, Zhao Y, et al. Enhanced low-temperature activity of CO2 methanation over highly-dispersed Ni/TiO2 catalyst. Catal Sci Technol 2013;3:2627–33.

[39] Lin W, Cheng H, He L, Yu Y, Zhao F. High performance of Ir-promoted Ni/TiO2 catalyst toward the selective hydrogenation of cinnamaldehyde. J Catal 2013;303:110–6.

[40] Ibrahim AA, Al-Fatesh AS, Khan WU, Soliman MA, Al Otaibi RL, Fakeeha AH. Influence of support type and metal loading in methane decomposition over iron catalyst for hydrogen production. J Chinese Chem Soc 2015;62:592–9.

[41] Huynh HL, Zhu J, Zhang G, Shen Y, Tucho WM, Ding Y, et al. Promoting effect of Fe on supported Ni catalysts in CO2 methanation by in situ DRIFTS and DFT study. J Catal 2020;392:266–77.

[42] Mihaylov M, Hadjiivanov K, Knözinger H. Formation of Ni(CO)4 during the interaction between CO and silica-supported nickel catalyst: An FTIR spectroscopic study. Catal Letters 2001;76:59–63.

[43] Bartholomew CH, Pannell RB. The stoichiometry of hydrogen and carbon monoxide chemisorption on alumina- and silica-supported nickel. J Catal 1980;65:390–401.

[44] Palazzolo A, Poucin C, Freitas AP, Ropp A, Bouillet C, Ersen O, Carenco S. The delicate balance of phase speciation in bimetallic nickel cobalt nanoparticles, Nanoscale 2022;14:7547-7560.

[45] Nguyen AM, Bahri M, Dreyfuss S, Moldovan S, Miche A, Méthivier C, Ersen O, Mézailles N, Carenco S. Bimetallic Phosphide (Ni,Cu)2P Nanoparticles by Inward Phosphorus Migration and Outward Copper Migration, Chem. Mater. 2019; 31(16):6124-6134.

[46] Kong X, Zheng R, Zhu Y, Ding G, Zhu Y, Li YW. Rational design of Ni-based catalysts derived from hydrotalcite for selective hydrogenation of 5-hydroxymethylfurfural. Green Chem 2015;17:2504–14.

[47] Kim SM, Abdala PM, Margossian T, Hosseini D, Foppa L, Armutlulu A, et al. Cooperativity and dynamics increase the performance of NiFe dry reforming catalysts. J Am Chem Soc 2017;139:1937–49.

[48] Yu W, Xiong K, Ji N, Porosoff MD, Chen JG. Theoretical and experimental studies of the adsorption geometry and reaction pathways of furfural over FeNi bimetallic model surfaces and supported catalysts. J Catal 2014;317:253–62.

CReDiT Author statement:

Martyna Przydacz: Literature search, Investigation, Data analysis, Writing - Original draft preparation. **Marcin Jędrzejczyk:** Literature search, Investigation, Data analysis. **Jacek Rogowski:** Investigation, Data analysis. **Dris Ihiawakrim:** Investigation, Data analysis. **Nicolas Keller:** Investigation, Data analysis, Writing - Original draft preparation, Writing – revised manuscript preparation. **Agnieszka M. Ruppert:** Conceptualization, Literature search, Resources, Methodology, Data analysis, Writing - Original draft preparation, Writing – revised manuscript preparation, Funding acquisition, Project administration, Supervision.

All authors read and approved the final manuscript.